Iron oxidation state of $FeTiO_3$ under high pressure

X. Wu,[1,*] G. Steinle-Neumann,[1] O. Narygina,[1] I. Kantor,[1,2] C. McCammon,[1] S. Pascarelli,[3] G. Aquilanti,[3] V. Prakapenka,[2] and L. Dubrovinsky[1]

[1]*Bayerisches Geoinstitut, Universität Bayreuth, Bayreuth D-95440, Germany*

[2]*CARS, University of Chicago, Chicago, Illinois 60437, USA*

[3]*European Synchrotron Radiation Facility, 38043 Grenoble, France*

(Received 16 June 2008; revised manuscript received 2 December 2008; published 11 March 2009)

The oxidation state of iron in $FeTiO_3$ under high pressure was investigated by combining x-ray diffraction, Mössbauer spectroscopy, x-ray-absorption spectroscopy, and density-functional theory based calculations. Our results demonstrate that the ilmenite-to-perovskite phase transition occurs above 20 GPa at room temperature and on compression two phases coexist to 40 GPa. The $Fe^{3+}/\Sigma Fe$ ratio increases up to 16 GPa, probably attributed to the *d*-electron drifting of cations via the oxygen bridge in the adjacent octahedral, then decreases at higher pressure due to the ilmenite-to-perovskite phase transition accompanied by a slight decrease in iron valence state. Our *ab initio* calculations further show that the most significant changes in the charge distribution in $FeTiO_3$ are associated with Ti and O.

DOI: 10.1103/PhysRevB.79.094106 PACS number(s): 61.05.cj, 61.50.Ks, 76.80.+y

I. INTRODUCTION

The structural, electronic, and magnetic properties of $FeTiO_3$ are of great interest in the materials and earth sciences. Ilmenite is a wide-band-gap semiconductor with a 2.5 eV band gap,[1] which is exploited to realize multifunctional devices.[2] Natural ilmenite is a common mineral found in metamorphic and igneous rocks on earth and also on the surface of the moon.[3,4] Iron oxidation states in $FeTiO_3$ can provide significant information about the weathering history of deposited minerals and the temperature and oxygen fugacity of the earth's mantle.[5]

At ambient conditions the nominal valence states of Fe and Ti in ilmenite have been extensively studied by various experimental methods and theoretical calculations.[6–11] There are two possible configurations: $Fe^{2+}Ti^{4+}$ and $Fe^{3+}Ti^{3+}$. Both configurations have been reported in natural ilmenite and synthetic samples.[7,8,11] Some synthetic samples, however, only show the $Fe^{2+}Ti^{4+}$ configuration.[6,10] One possible reason is that the presence of hematite in natural ilmenite[7,8] leads to the recording of "artificially" mixed-valence signatures; another is probably the different synthesis conditions, such as sintering temperature, oxygen fugacity, and quenching time.

The ilmenite structure is based on a hexagonal-close-packed oxygen lattice with metal atoms (Fe and Ti) occupying two-thirds of the available octahedral sites. Each octahedron shares three edges with octahedra inside the layer, a face with an octahedron of the second type of cation in the adjacent layer, and the opposite face with a vacant octahedral site [Fig. 1(a)]. In other words, layers of Fe and Ti alternate with a cation ordering of Ti-Fe-*V*-Fe-Ti (*V*: vacant sites) along the *c* axis [Fig. 1(a)]. Therefore, along the *c* axis a metal-metal intervalence charge transfer is expected when external pressure is applied. Indeed, under high pressure a large intervalence charge transfer from $Fe^{2+}+Ti^{4+}$ to $Fe^{3+}+Ti^{3+}$ was reported in natural ilmenite by *in situ* Mössbauer spectroscopy.[8] However these observations are in conflict with previous Mössbauer experiments on synthetic $FeTiO_3$ up to 17 GPa.[6] Recent x-ray-diffraction investigations of the electron-density distribution of single-crystal $FeTiO_3$ ilmenite have shown neither charge transfer nor electron hopping between Fe and Ti atoms along the *c* axis under high pressures.[12,13] Similarly, theoretical calculations do not support an increase in the amount of Fe^{3+} for ilmenite at high pressure,[14] but early molecular-orbital calculations imply that the $Fe^{2+}+Ti^{4+}$ to $Fe^{3+}+Ti^{3+}$ charge transfer could occur by Fe-Ti bonding across shared polyhedral edges.[15] This implies that there is currently no consensus on the existence and possible mechanism of pressure-induced charge transfer for ilmenite.

Related and in addition to charge transfer under pressure, the question of phase transitions in the system has been subject of current debate. Three polymorphs of $FeTiO_3$ have been reported at high pressure—ilmenite, the lithium niobate (LN), and the perovskite (Pv) structure.[12,13,16–18] LN has been shown to be a metastable phase that nevertheless can be stabilized to ambient conditions.[17,18] Its structure is similar to that of ilmenite, but cations order along the *c* axis. Figure 1(b) shows that FeO_6 octahedra share not only faces but also edges with TiO_6 octahedra. In perovskite structured $FeTiO_3$ [Fig. 1(c)], Fe cations are surrounded by 8+4 oxygen anions

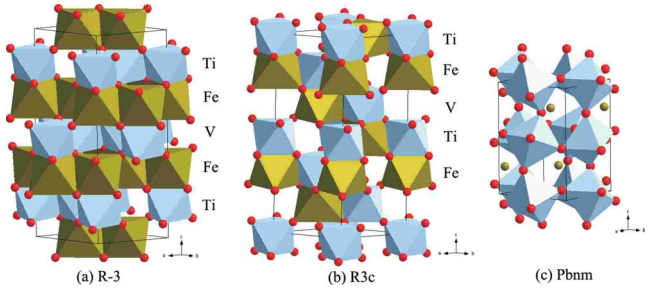

FIG. 1. (Color online) The crystal structures of $FeTiO_3$ polymorphs: (a) ilmenite (space group *R*-3), (b) lithium niobate (*R*3*c*), and (c) perovskite (*Pbnm*). Ti-coordinated oxygen octahedra are indicated in blue, while Fe atoms or Fe-coordinated oxygen octahedra are shown in brown.

in the distorted dodecahedral coordination and TiO_6 octahedra share corners in three dimensions. To the best of our knowledge, there is no information on iron oxidation states in the LN or Pv phases available, although no changes in valence state of Fe or Ti are expected for the ilmenite-to-perovskite transition, based on the measured volume changes.[17] In this paper we shed light on the valence state of iron in $FeTiO_3$ up to 53 GPa by means of Mössbauer spectroscopy (MS), x-ray-absorption spectroscopy (XAS), x-ray powder diffraction (XRD), and density-functional theory (DFT) based electronic structure calculations.

II. METHODS

A. Experiment

The ilmenite $FeTiO_3$ sample was synthesized by standard solid-state reaction. Stoichiometric amounts of ^{57}Fe(95.38%), Fe_2O_3(99.998%), and TiO_2(99.998%) were mixed and ground under ethanol in an agate mortar. The mixture was loaded into a sealed and evacuated silica tube, which was heated at 1200 °C for 24 h. Then it was quenched to ambient conditions. The product was examined by XRD and MS, which confirmed a single phase (ilmenite) without any impurity.

For high-pressure studies we used a four-pin modified Merrill-Basset design diamond-anvil cell (DAC) with 300 μm culets. A 150-μm-diameter hole was drilled in the rhenium gasket that was preindented to 30–40 μm. In different runs NaCl, LiF, or liquid Ne were used as pressure-transmitting media. A small ruby sphere was loaded for pressure calibration, according to its R_2 fluorescence peak position.[19]

The *in situ* XRD measurements up to 47 GPa were carried out at beamline 13-BMD of the Advanced Photon Source (APS). Data were collected with a MAR345 detector using a x-ray beam with wavelength of 0.3344 Å and a beam size of 5×5 μm^2. Additional detail XRD experiments up to 20 GPa for obtaining the unit-cell parameters were carried out at Bayerisches Geoinstitut (BGI) using a system consisting of high-brilliance FRD rotating anode generator and Bruker APEX charge-coupled device area detector. The Mo $K\alpha$ radiation ($\lambda=0.7108$ Å) was focused to about $\varnothing50$ μm full width at half maximum (FWHM) beam size. Collecting time of each pattern was 15 min. All collected images were integrated using the FIT2D program in order to obtain conventional one-dimensional diffraction spectra. X-ray appearance near-edge structure (XANES) spectra of Fe K edge were recorded at the energy dispersive XAS beamline ID24 of the European Synchrotron Radiation Facility (ESRF).[20] The x-ray beam with an energy window around the Fe K edge was focused both in the horizontal and vertical planes to reach a 5×5 μm^2 spot, and pixel-energy calibration was obtained by measuring spectra on a reference Fe foil sample. The XANES spectra were treated using the VIPER software.[21] ^{57}Fe Mössbauer spectra were measured in a transmission mode on a constant acceleration Mössbauer spectrometer using a high specific activity ^{57}Co point source in a Rh matrix. The velocity scale was calibrated relative to a 25-μm-thick α-Fe foil. Collection time for each spectrum was at least 8 h. Mössbauer spectra were fitted to Lorentzian line shapes using the commercial software NORMOS written by R. A. Brand (distributed by Wissenschaftliche Elektronik GmbH, Germany).

B. Calculations

We performed the first-principles calculations based on density-functional theory as implemented in the WIEN2K code.[22,23] All unit-cell parameters of ilmenite, LN, and Pv structural models[16,17] were optimized according to the minimum total energy. For ilmenite we considered both the ferromagnetic state and an antiferromagnetic configuration found stable in ilmenite,[9] in which the Fe^{2+} spins are ferromagnetically aligned within a bilayer but antiferromagnetically coupled between bilayers: no differences in magnetic moment and electron charge of iron were found between the magnetic configurations. Thus we restricted ourselves to ferromagnetic configurations in the calculations for the LN and Pv phases.

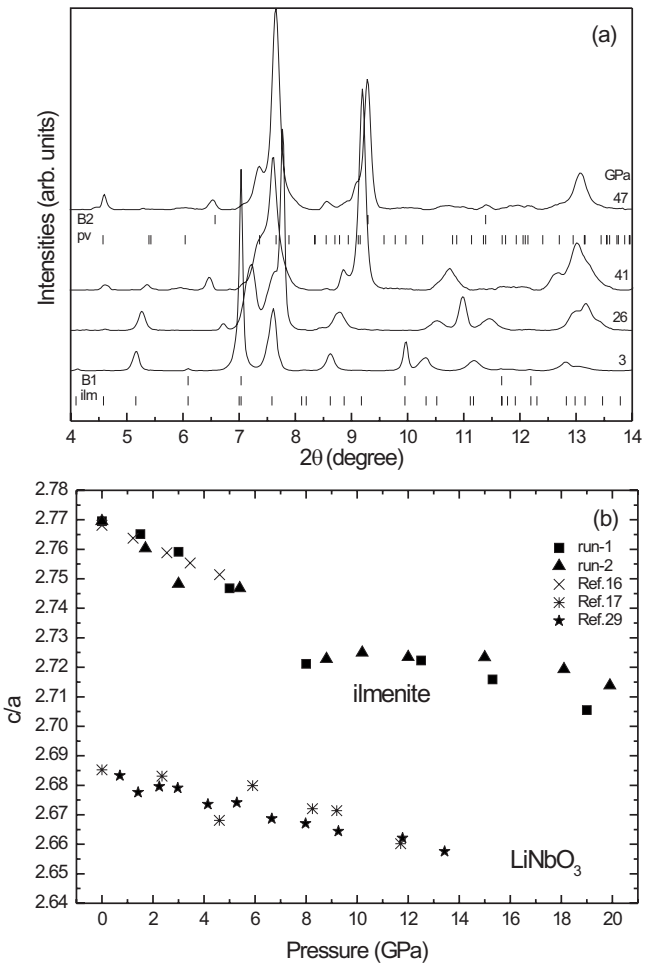

FIG. 2. (a) Selected synchrotron radiation x-ray-diffraction patterns of $FeTiO_3$ at high pressure with the background subtracted. Vertical bars represent the positions of diffraction peaks which are assigned to the different phases, NaCl (B1: $Fm3m$; B2: $Pm3m$) and $FeTiO_3$ (ilm: R-3; pv: $Pbnm$). (b) The c/a ratio for the ilmenite and the LN in $FeTiO_3$ vs pressure.

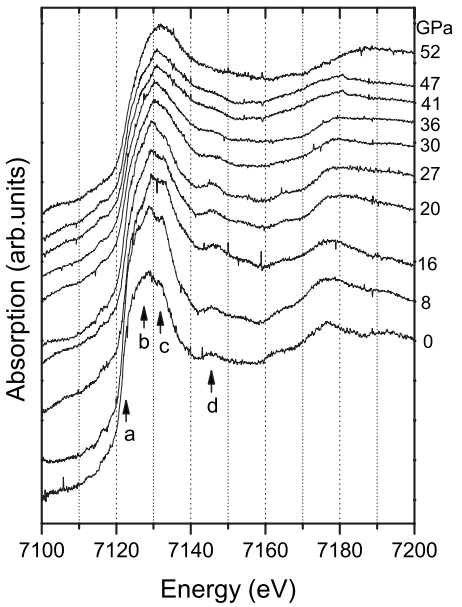

FIG. 3. Fe *K*-edge XANES spectra at various pressures.

We used these optimized structural models to calculate electronic charges of the atoms by topological analysis of Bader[24] of the charge density [atoms in molecules (AIM) theory]. In order to allow for an accurate comparison we used the same muffin-tin radius (R_{MT}) for the same kind of atom in all calculations. R_{MT} for Fe, Ti, and O were chosen as 1.7, 1.5, and 1.8 bohr, respectively. We treated Fe and Ti with an Ar core and O with a He core, and for all valence states we used augmented plane wave plus local orbitals in the basis set. We set a plane-wave expansion with $R_{MT}K_{max}=7.0$, and reciprocal space was sampled with a 500 *k*-point mesh in the full Brillouin zone. The self-interaction corrected (SIC) generalized gradient approximation plus Hubbard U (GGA+*U*) method was used for the exchange-correlation energy.[25] In our calculations we adopted $U=8$ eV and $J=0.95$ eV for both Fe and Ti, consistent with other work in the system and other transition-metal-based oxides.[26–28] AIM

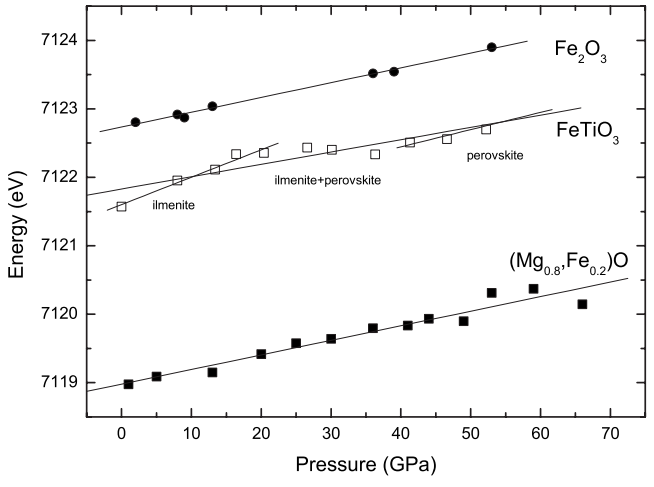

FIG. 4. The pressure dependence of the energy of Fe *K*-edge absorption (E_K). The data of Fe_2O_3 and $(Mg_{0.8},Fe_{0.2})O$ are from Ref. 35.

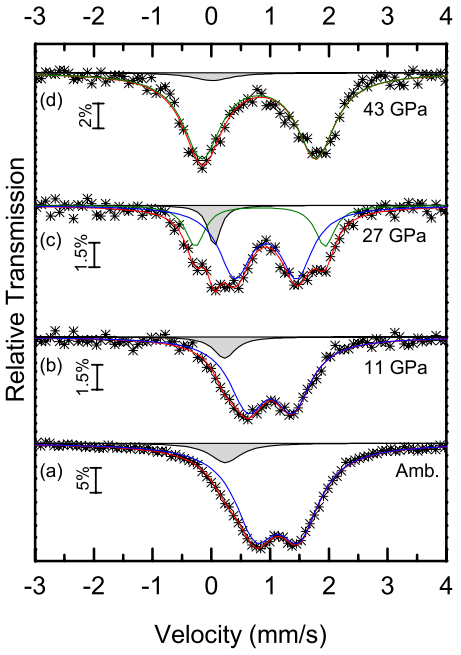

FIG. 5. (Color online) Typical ^{57}Fe Mössbauer spectra of $FeTiO_3$ at high pressure. (a) The spectrum was recorded at ambient condition without diamond-anvil cell. [(b)–(d)] Spectra collected in DAC with Ne as pressure-transmitting medium. The gray fraction indicates the Fe^{3+} component.

requires a smooth charge density ρ across the atomic sphere boundary, with a high-order spherical harmonics (l) expansion up to $l=8$ or 10. We tested all candidate phases and found no difference to within 0.002 electron for $l=6$ and $l=8$. Therefore, an expansion up to $l=6$ and no symmetry restrictions were used in the AIM calculations.

III. RESULTS

A. Experimental

Synchrotron radiation XRD data of $FeTiO_3$ were collected at pressures of up to 47 GPa at room temperature. In Fig. 2(a) several selected XRD patterns are shown, which illustrates that the perovskite phase appears above 20 GPa and the ilmenite phase persists to 41 GPa. As previously shown the LN phase is metastable[17,18] and transforms to the perovskite structure above 16 GPa.[17] In order to evaluate the possibility of its existence in our experiments, conventional XRD experiments up to 20 GPa were performed using Ne as pressure-transmitting media to investigate structural properties in detail by extracting the unit-cell parameters using a full-profile refinement (Le Bail method). The powder XRD patterns of both ilmenite and LN are very similar because of their similar structures [Figs. 1(a) and 1(b)], but the c/a ratio of the LN phase is considerably smaller than that of ilmenite.[18] In our data sets the c/a ratio is larger than that of the LN phase from previous studies[17,29] for all pressures [Fig. 2(b)], implying that the LN phase does not occur in our experiments. In addition, a post-perovskite phase of $FeTiO_3$ predicted above 44 GPa (Ref. 14) is not observed in our experiments.

TABLE I. Iron hyperfine parameters in $FeTiO_3$ under pressure. I: recorded at ambient conditions without diamond-anvil cell; II: measured in a Ne pressure-transmitting medium; III: measured in a LiF pressure-transmitting medium. The numbers in parentheses are the estimated standard deviations in units of the last digit based on fitting statistics. For reference values from the literature for $FeTiO_3$ ilmenite (ilm) at zero pressure are included. Mössbauer parameters for Fe^{2+} in octahedral coordination in $(Mg_{0.8}Fe_{0.2})O$ (ferropericlase, fp) and dodecahedral coordination in $(Mg_{0.88}Fe_{0.12})SiO_3$ perovskite (pv) are given for comparison.

		Octahedral Fe^{2+}				Fe^{3+}			Dodecahedral Fe^{2+}			
	P (GPa)	δ (mm/s)	ΔE_Q (mm/s)	Γ (mm/s)	A (%)	δ (mm/s)	Γ (mm/s)	A (%)	δ (mm/s)	ΔE_Q (mm/s)	Γ (mm/s)	A (%)
I	0.0	1.12(1)	0.74(1)	0.86(1)	92(1)	0.23(2)	0.63(5)	8(1)				
II	8	1.02(2)	0.77(3)	0.68(5)	95(5)	0.18(7)	0.3(1)	5(3)				
	12	1.00(2)	0.77(2)	0.74(3)	91(4)	0.22(3)	0.4(1)	9(3)				
	14	1.00(1)	0.80(2)	0.78(3)	87(3)	0.17(3)	0.57(8)	13(3)				
	18	0.97(9)	0.96(1)	0.77(2)	90(2)	0.06(2)	0.55(7)	10(2)				
	21	0.94(5)	0.97(1)	0.68(2)	75(2)	0.06(1)	0.5(1)	9(1)	0.88(2)	2.00(5)	0.49(5)	16(2)
	27	0.92(2)	1.05(4)	0.66(4)	67(6)	0.05(2)	0.26(6)	8(2)	0.83(1)	2.21(3)	0.40(6)	25(5)
	30	0.89(8)	1.10(3)	0.63(3)	56(4)	0.07(3)	0.39(7)	6(1)	0.87(6)	2.13(2)	0.49(3)	38(4)
	37	0.86(2)	1.12(6)	0.59(4)	38(3)	0.03(3)	0.3(1)	5(2)	0.81(1)	2.12(3)	0.57(4)	57(4)
	43					0.01(5)	0.80(6)	5(3)	0.80(1)	1.94(2)	0.78(3)	95(4)
III	0	1.06(3)	0.81(4)	0.56(7)	96(1)	0.23(5)	0.44(8)	4(1)				
	5	1.04(9)	0.98(1)	0.73(2)	96(3)	0.12(3)	0.3(1)	4(2)				
	10	1.07(4)	0.98(6)	0.71(8)	89(1)	0.13(1)	0.53(3)	11(1)				
	11	1.05(6)	1.07(1)	0.69(2)	88(2)	0.09(1)	0.48(5)	12(1)				
	15	1.04(3)	1.11(5)	0.71(7)	88(1)	0.05(7)	0.47(2)	12(1)				
	22	0.99(5)	1.26(2)	0.58(2)	49(3)	0.07(2)	0.40(4)	9(1)	0.93(6)	2.23(2)	0.57(3)	42(4)
	31	0.91(3)	1.26(6)	0.57(7)	39(1)	0.01(5)	0.41(2)	10(1)	0.86(2)	2.22(5)	0.52(6)	51(1)
	39	0.90(3)	1.30(5)	0.64(8)	38(1)	−0.03(4)	0.39(1)	9(1)	0.85(2)	2.32(5)	0.55(6)	53(1)
ilm[a]	0	1.04	0.88		100							
ilm[b]	0	1.06(1)	0.69(1)		74.2	0.27(2)	0.32(1)	16.1				
fp[c]	0	1.03	0.93		100							
pv[d]	0					0.13(6)	0.45(4)	5(3)	1.15(2)	1.90(3)		95(2)

[a]Reference [6].
[b]Reference [8].
[c]Reference [35].
[d]Reference [36].

The results from XRD provide the basis for the analysis and discussion of high-pressure XANES and MS spectra of $FeTiO_3$. Fe K-edge XANES spectra collected at high pressure are shown in Fig. 3. Generally, the Fe K absorption edge comprises three features caused by electron transitions to bound states: pre-edge ($1s \rightarrow 3d$), shoulder ($1s \rightarrow 4s$), and edge crest ($1s \rightarrow 4p$). The pre-edge is often used to determine Fe oxidation state and coordination number according to the position of its centroid and its integrated intensity.[30–32] Unfortunately, we did not observe clear pre-edge peaks in our experiments. Upon compression and at least up to 16 GPa, the peaks of the XANES spectra (labeled b, c, and d in Fig. 3) shift to higher energy. In general this is related to a decrease in nearest-neighbor distances upon compression. This trend is interrupted near 20 GPa where the "d" peak shifts toward lower energy, most probably indicating an increase in the Fe-O bond length. This effect can be interpreted by the presence of a crystal phase with higher Fe coordination, in agreement with the XRD results.

The position of the absorption edge (E_K) ("a" in Fig. 3) is also sensitive to changes in the valence state and chemical bonding of the absorbing atom.[33–35] Here we used the maximum of the first derivative ($\partial\mu/\partial E$) as the E_K value. Figure 4 shows E_K as a function of pressure, compared to E_K of Fe_2O_3 and $(Mg_{0.8},Fe_{0.2})O$.[35] The E_K of $FeTiO_3$ is close to that of Fe_2O_3, mostly attributed to their similar chemical-bonding environment. In Fe_2O_3 and $(Mg_{0.8}Fe_{0.2})O$ structure and valence do not change up to a pressure of 70 GPa and the slopes of E_K for these two compounds remain constant as a function of pressure and the trends are parallel (Fig. 4). E_K for $FeTiO_3$ shows a similar overall slope with pressure (Fig. 4), indicating that no big change in Fe valence occurs.

In detail, however, three different regions in the pressure slope can be identified, correlated with the phase transition in the system as established by XRD: at pressures below 20 and above 40 GPa E_K increases linearly, indicating a single phase being present in the cell. In the intermediate pressure regime

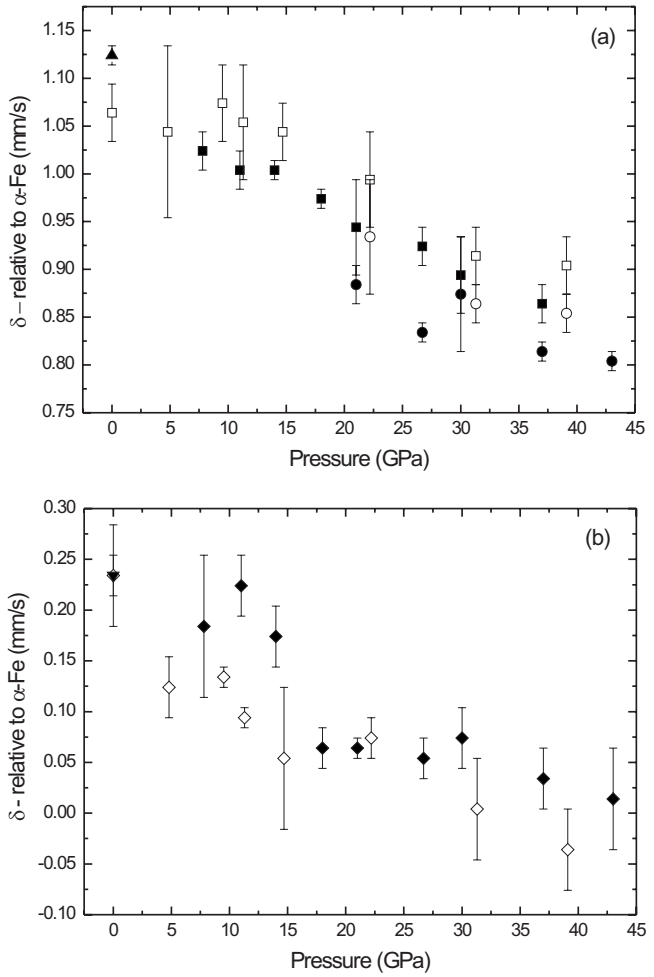

FIG. 6. The isomer shift of the (a) ferrous and (b) ferric components vs pressure. Open symbols: data measured in Ne pressure-transmitting medium; solid symbols: data measured in LiF pressure-transmitting medium. Triangles: data recorded at ambient conditions without diamond-anvil cell. Squares: Fe^{2+} component in the ilmenite phase; circles: Fe^{2+} component in the perovskite phase; diamonds: Fe^{3+} component.

E_K is near constant due to the coexistence of the two phases: ilmenite and Pv-structured $FeTiO_3$.

We performed two sets of MS measurements up to 43 GPa at room temperature using LiF and liquid Ne as pressure media. Several spectra are shown in Fig. 5. At ambient conditions the spectrum shows a well-resolved doublet attributed to a Fe^{2+} component and a Fe^{3+} singlet [Fig. 5(a)]. With increasing pressure a new doublet appears [Fig. 5(c)]. Above 40 GPa the spectra consist of only one well-resolved doublet and a singlet. Hyperfine parameters (isomer shift δ and quadrupole splitting ΔE_Q) are listed in Table I and plotted in Fig. 6 as function of pressure. For the Fe^{2+} component in ilmenite we find δ=1.12 mm/s and ΔE_Q=0.74 mm/s, consistent with values reported in the literature for $FeTiO_3$ ilmenite[6,8] and similar to (Mg,Fe)O with sixfold coordinated Fe^{2+} (Table I). The Fe^{2+} component of the new doublet [Fig. 5(c)] with δ=0.83 mm/s and ΔE_Q=2.21 mm/s is consistent with that of $(Mg_{0.9},Fe_{0.1})SiO_3$ (Ref. 36) in the perovskite structure (Table I), assigned to dodecahedrally coordinated Fe^{2+}. The

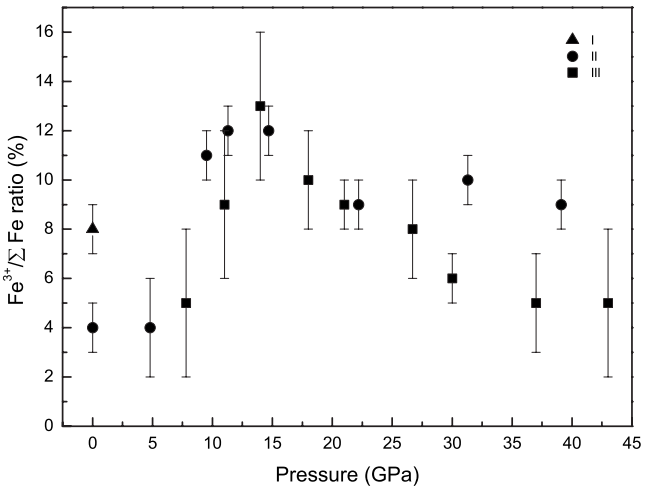

FIG. 7. The $Fe^{3+}/\Sigma Fe$ ratio at various pressures. I: recorded at ambient conditions without diamond-anvil cell; II: measured in Ne pressure-transmitting medium; III: measured in LiF pressure-transmitting medium.

isomer shift of all three types of Fe components decreases with increasing pressure, attributed to the *s*-electron density increasing at the Fe nucleus. δ for Fe^{2+} in the perovskite phase is smaller than that in the ilmenite phase at the same pressure due to the different coordination environment of iron. However the effect of pressure on the quadrupole splitting of the Fe^{2+} component in ilmenite is significant (Table I). The coexistence range of Fe^{2+} in both octahedral and dodecahedral environments agrees well with that of the ilmenite and perovskite phases observed by XRD. Table I and Fig. 7 show that the relative Fe^{3+} content increases slightly from 6% (the mean value) at 0 GPa to 13% at 14 GPa, then decreases at higher pressure.

B. Calculations

Figure 8 shows the charges of Fe, Ti, and O at various

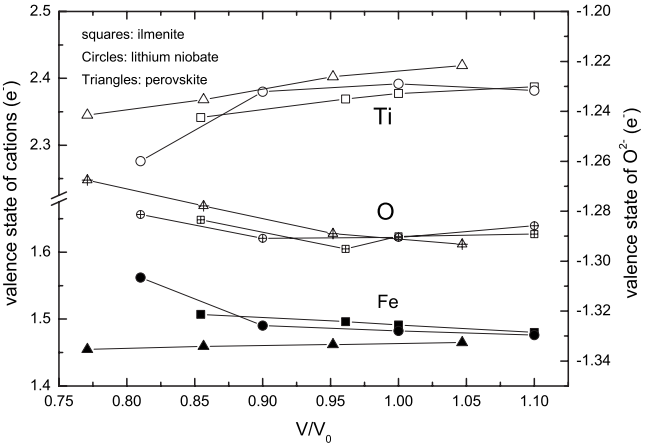

FIG. 8. The charge valence states computed for Fe, Ti, and O as a function of compression (V/V_0). For V_0 we used the experimental data (Refs. 16 and 17). Cation valence is given by the left coordinate axis, while those of the oxygen ion are on the right coordinate axis.

volumes calculated according to the topological analysis of Bader.[24] The charges of O^{2-} are between −1.26 and −1.30, which is close to the reference charge of pure ionic O^{2-} (−1.46 *e*).[37] For ilmenite at V_0 the charges of Fe, Ti, and O (1.48, 2.35, −1.29) are similar to the results obtained using Mulliken population analysis (1.74, 2.32, and −1.36, respectively).[9] Upon compression, the charge of Fe in ilmenite increases slightly and that of lithium niobate increases significantly for $V/V_0 < 0.9$, but the corresponding pressures are out of the stability range of the LN phase. In Pv-structured $FeTiO_3$ the Fe charge is almost constant and it is slightly smaller than in the ilmenite or LN phase. It indicates that the relative Fe^{3+} content in the perovskite phase is less than that of ilmenite phase. Considering the comparison of the valence states of Fe, Ti, and O in the three phases, the main changes in distribution of charges are related to transfer of electron density between Ti and O, while changes on Fe are secondary.

IV. DISCUSSION

While we observe only a small change in Fe^{3+} content in our MS experiments (up to 15% near 12 GPa), a large increase in ferric iron from 13% at 0 GPa to 30% at 14 GPa in ilmenite was reported previously.[8] The initial Fe^{3+} in Ref. 8 is consistent with other studies using natural samples[7] and could stem from the fact that in natural samples $FeTiO_3$ coexists with Fe_2O_3, forming a solid solution via the coupled substitution $2Fe^{3+}=Fe^{2+}+Ti^{4+}$. Although a Mössbauer study of the $(1-x)Fe_2O_3$-$xFeTiO_3$ series shows that no electron transfer occurs between Fe^{2+} and Fe^{3+} in the range $0.75 < x < 1.0$ at ambient conditions,[38] charge transfer could occur at pressure. This notion finds support in the study of cation ordering in synthetic $0.65(FeTiO_3)0.35(Fe_2O_3)$ by time-of-flight neutron diffraction;[39] under compression the cation-cation interaction is enhanced, leading to an increase of cation ordering. This cation ordering in the $FeTiO_3$-Fe_2O_3 solid solution could result in a steep initial increase in the $Fe^{3+}/\Sigma Fe$ ratio and a subsequent saturation when the ions are well ordered, as observed in experiments up to 2 and above 4 GPa, respectively.[8]

Despite the limited extent of charge transfer observed here the transfer mechanism is of great importance. Two principal possibilities exist in the ilmenite structure (Figs. 1 and 9): either across the shared faces of Fe and Ti octahedra or through indirect exchange via the O^{2-} anions. Molecular-orbital calculations based on a $(FeTiO_{10})^{14-}$ cluster[15] suggest that the $Fe^{2+}+Ti^{4+}$ to $Fe^{3+}+Ti^{3+}$ charge transfer is facilitated through shared Fe-Ti polyhedral faces. This is in contrast to a recent maximum entropy method (MEM) analysis of single-crystal XRD intensities:[13] the measurements show a decrease in charge density along the direct Fe-Ti connection as a function of pressure, making charge transfer via this route highly unlikely. However, the same measurements show an increase in charge density between both Fe-O and Ti-O in ilmenite with pressure, attributed to the decreased bond length. In this case the *d* electrons of the cations in the octahedral environment transfer charge from the t_{2g} orbital of one cation to the t_{2g} orbitals of the neighboring cations through the p_π orbitals of the O^{2-} ion.[40]

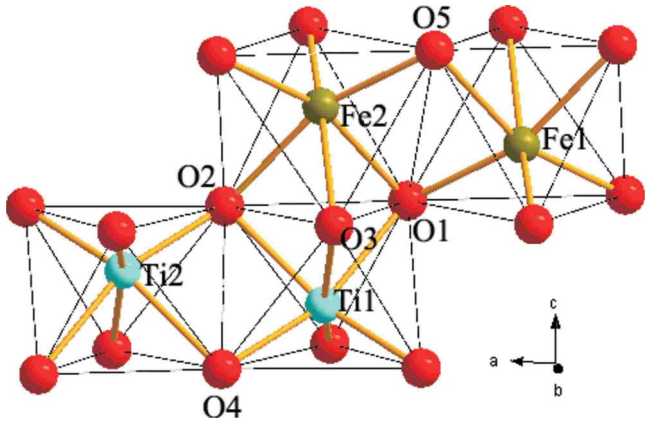

FIG. 9. (Color online) A fragment of the ilmenite structure. The bond lengths between cations and the oxygen ion shared on a shared face are longer than those between cations and the oxygen ion not on a common face.

Bond lengths for both Ti-O and Fe-O decrease due to compression and the decreasing c/a ratio as discussed above (Fig. 2). For charge transfer via the O^{2-} anions two routes are possible (Fig. 9): Ti1-O1-Fe1 or Ti1-O1-Fe2. As the bond length between Fe1-O1 is shorter than between Fe2-O1 (at ambient pressure by 0.12 Å), charge transfer via Ti1-O-Fe1 appears more likely.

By looking in detail at the structure of the clusters for the molecular-orbital computations the discrepancy with the experiments performed here as well as previous[6] and current computations can be understood readily: the cluster geometry in Ref. 15 is similar to the LN, but not the ilmenite structure. Moreover, indeed, for our computations in the LN geometry we do observe a significant charge transfer for $V/V_0 < 0.9$ (outside the pressure range where the LN phase of $FeTiO_3$ can be stabilized).

The charge-transfer mechanism between Fe and Ti proposed here via the O^{2-} anions puts the interlayer charge transfer on equal footing to the charge-transfer mechanism responsible for increased electrical conductivity under pressure.[12,13] Electrical conductivity in $FeTiO_3$ ilmenite is highly anisotropic, with conductivity strongly enhanced in the *a*-*b* plane. As the Ti-(Fe-) octahedra share only edges in the basal plane and cations are at large distances (Figs. 1 and 9, ~3.0 Å), electrical conductivity can only be facilitated through the O^{2-} anions. Here again, Fe-O and Ti-O distances decrease under pressure, enhancing the electrical conductivity.

Based on ionic radii systematics[41] the volume change at the ilmenite-to-perovskite transition was estimated to be 3.3 % for $Fe^{2+}Ti^{4+}O_3$ and 5.0% for $Fe^{3+}Ti^{3+}O_3$.[17] Previous experimental data of the volume change show $2.8 \pm 0.3\%$ (Ref. 17) and in computations it is estimated as 1.5% (Refs. 9 and 14) at the phase-transition boundary. Due to insufficient number of data points we are not able to independently estimate a volume change from our experiments. This implies that the $Fe^{3+}Ti^{3+}$ configuration is unlikely in the perovskite structure. This is consistent with the behavior of iron charge computed here (Fig. 8), where a decrease in iron charge appears from ilmenite to Pv. Similarly, the *s*-electron density at

the Fe nucleus in the perovskite phase is slightly larger than that in the ilmenite phase based on the corresponding isomer shifts (Fig. 6 and Table I).

V. CONCLUSION

The electronic oxidation state of iron in $FeTiO_3$ has been studied as a function of pressure using Mössbauer spectroscopy, x-ray-absorption spectroscopy, and DFT based calculations. All experimental results verify that there is a phase transition from ilmenite to perovskite around 20 GPa and the pressure range of two phases coexisting is from 20 to 40 GPa on compression at ambient temperature. The isomer shift of Fe^{2+} in the dodecahedrally coordinated environment of the perovskite phase is smaller than that in the octahedral environment of the ilmenite phase at the same pressure. The $Fe^{3+}/\Sigma Fe$ ratio increases slightly with pressure and reaches a maximum of 13% around 16 GPa. All experimental and computational evidence supports the conclusion that the dominant oxidation state of Fe remains ferrous in the perovskite phase.

ACKNOWLEDGMENTS

The authors would like to thank L. Rose-Weston for her help in sample synthesis. X.W. is grateful for support from Alexander von Humboldt Foundation.

*Corresponding author; xiang.wu@uni-bayreuth.de

[1] D. S. Ginley and M. A. Butler, J. Appl. Phys. **48**, 2019 (1977).
[2] H. Hojo, K. Fujita, K. Tanaka, and K. Hirao, Appl. Phys. Lett. **89**, 142503 (2006).
[3] S. E. Haggerty and V. Sautter, Science **248**, 993 (1990).
[4] K. N. Raymond and H. R. Wenk, Contrib. Mineral. Petrol. **30**, 135 (1971).
[5] D. H. Lindsley, Year Book - Carnegie Inst. Washington **62**, 60 (1963).
[6] R. W. Vaughan and H. G. Drickamer, J. Chem. Phys. **47**, 1530 (1967).
[7] P. A. van Aken, B. Liebscher, and V. J. Styrsa, Phys. Chem. Miner. **25**, 323 (1998).
[8] T. Seda and G. R. Hearne, J. Phys.: Condens. Matter **16**, 2707 (2004).
[9] N. C. Wilson, J. Muscat, D. Mkhonto, P. E. Ngoepe, and N. M. Harrison, Phys. Rev. B **71**, 075202 (2005).
[10] G. Radtke, S. Lazar, and G. A. Botton, Phys. Rev. B **74**, 155117 (2006).
[11] T. Fujii, M. Yamashita, S. Fujimori, Y. Saitoh, T. Nakamura, K. Kobayashi, and J. Takada, J. Magn. Magn. Mater. **310**, e555 (2007).
[12] T. Yamanaka, J. Synchrotron Radiat. **12**, 566 (2005).
[13] T. Yamanaka and Y. Komatsu, Phys. Chem. Miner. **34**, 307 (2007).
[14] N. C. Wilson, S. P. Russo, J. Muscat, and N. M. Harrison, Phys. Rev. B **72**, 024110 (2005).
[15] D. M. Sherman, Phys. Chem. Miner. **14**, 364 (1987).
[16] B. A. Wechsler and C. T. Prewitt, Am. Mineral. **69**, 176 (1984).
[17] K. Leineweber, W. Utsumi, Y. Tsuchida, T. Yagi, and K. Kurita, Phys. Chem. Miner. **18**, 244 (1991).
[18] L. C. Ming, Y. H. Kim, T. Uchida, Y. Wang, and M. Rivers, Am. Mineral. **91**, 120 (2006).
[19] H. K. Mao, J. Xu, and P. M. Bell, J. Geophys. Res. **91**, 4673 (1986).
[20] S. Pascarelli, O. Mathon, and G. Aquilanti, J. Alloys Compd. **362**, 33 (2004).
[21] K. V. Klementiev, VIPER for Windows, freeware, www.desy.de/~klmn/viper.html; K. V. Klementev, J. Phys. D: Appl. Phys. **34**, 209 (2001).
[22] P. Blaha, K. Schwarz, G. K. H. Madsen, D. Kvasnicka, and J. Luitz, *WIEN2k, An Augmented Plane Wave Local Orbitals Program for Calculating Crystal Properties* (Technische Universität Wien, Wien, Austria, 2002).
[23] K. Schwarz, P. Blaha, and G. K. H. Madsen, Comput. Phys. Commun. **147**, 71 (2002).
[24] R. F. Bader, *Atoms in Molecules: A Quantum Theory*, International Series of Monographs on Chemistry Vol. 22 (Oxford University Press, New York, 1994).
[25] V. I. Anisimov, I. V. Solovyev, M. A. Korotin, M. T. Czyzyk, and G. A. Sawatzky, Phys. Rev. B **48**, 16929 (1993).
[26] R. Pentcheva and H. S. Nabi, Phys. Rev. B **77**, 172405 (2008).
[27] G. K. H. Madsen and P. Novák, Europhys. Lett. **69**, 777 (2005).
[28] S. L. Dudarev, G. A. Botton, S. Y. Savrasov, C. J. Humphreys, and A. P. Sutton, Phys. Rev. B **57**, 1505 (1998).
[29] A. Mehta, K. Leineweber, A. Navrotsky, and M. Akaogi, Phys. Chem. Miner. **21**, 207 (1994).
[30] M. Wilke, F. Farges, P. Petit, G. E. Brown, and F. Martin, Am. Mineral. **86**, 714 (2001).
[31] A. J. Berry, H. O'Neill, K. D. Jayasuriya, S. J. Campbell, and G. J. Foran, Am. Mineral. **88**, 967 (2003).
[32] M. Wilke, F. Farges, G. M. Partzsch, C. Schmidt, and H. Behrens, Am. Mineral. **92**, 44 (2007).
[33] U. C. Srivastava and H. L. Nigam, Coord. Chem. Rev. **9**, 275 (1973).
[34] F. W. Lytle, R. B. Sandstorm, D. R. Marques, J. Wong, C. L. Spiro, G. P. Huffman, and F. E. Huggins, Nucl. Instrum. Methods Phys. Res. A **226**, 542 (1984).
[35] I. Kantor, L. Dubrovinsky, and C. A. McCammon, *Ferric Iron Determination at High Pressures Using Micro-XANES Analysis* (Bayerisches Geoinstitut, Bayreuth, Germany, 2005), pp. 165–167.
[36] O. V. Narygina, I. Yu. Kantor, X. Wu, S. Pascarelli, G. Aquilanti, C. McCammon, and L. S. Dubrovinsky, XNEAS study of spin crossover in Fe-bearing silicate pervoskite, Phase Transition (unpublished).
[37] R. Laskowski, P. Blaha, and K. Schwarz, Phys. Rev. B **67**, 075102 (2003).
[38] B. N. Warner, P. N. Shive, J. L. Allen, and L. Terry, J. Geomagn. Geoelectr. **24**, 353 (1972).
[39] R. J. Harrison, H. J. Stone, and S. A. T. Redfern, Phys. Earth Planet. Inter. **154**, 266 (2006).
[40] K. Kamata, T. Nakamura, and T. Sata, Bull. Tokyo Inst. Technol. **120**, 73 (1974).
[41] R. D. Shannon, Acta Crystallogr., Sect. A: Cryst. Phys., Diffr., Theor. Gen. Crystallogr. **32**, 751 (1976).